Lifetime measurements of normal deformed states in $^{165}_{71}$Lu

K. Andgren,[1,2,*] Zs. Podolyák,[1] A. Dewald,[3] F. R. Xu,[4] A. Algora,[5,6] M. Axiotis,[7] D. Bazzacco,[8] P. G. Bizzeti,[9] A. M. Bizzeti-Sona,[9] B. Cederwall,[2] G. de Angelis,[7] E. Farnea,[7] A. Fitzler,[10] A. Gadea,[7] W. Gelletly,[1] S. Lunardi,[8] O. Möller,[10] N. Marginean,[7] T. Martinez,[7] T. Pissulla,[10] C. Rusu,[7] C. A. Ur,[8] R. Venturelli,[8] P. M. Walker,[1] and C. Wheldon[1]

[1]*Department of Physics, University of Surrey, Guildford GU2 7XH, UK*
[2]*Department of Physics, Royal Institute of Technology, Stockholm, Sweden*
[3]*Institut für Kernphysik, Universität zu Köln, Zülpicher Str. 77, D-50937 Köln, Germany*
[4]*School of Physics, Peking University, Beijing, China*
[5]*IFIC, Valencia, Spain*
[6]*MTA, ATOMKI, Debrecen, Hungary*
[7]*I.N.F.N., Laboratori Nazionali di Legnaro, Legnaro, Italy*
[8]*Dipartimento di Fisica and I.N.F.N., Sezione di Padova, Padova, Italy*
[9]*Dipartimento di Fisica and I.N.F.N., Sezione di Firenze, Firenze, Italy*
[10]*Institut für Kernphysik, Universität zu Köln, Zülpicher Str. 77, D-50937 Köln, Germany*

(Received 8 October 2004; published 27 January 2005)

Picosecond lifetimes of medium spin states in ^{165}Lu were measured for the first time. The reaction used to populate the nucleus of interest was ^{139}La(^{30}Si, $4n$)^{165}Lu at a beam energy of 135 MeV. The beam was provided by the XTU-tandem accelerator of Laboratori Nazionali di Legnaro, Italy. By using the differential decay curve method, lifetimes of 19 states in four different rotational bands were obtained. Therefrom the $B(E2)$ values and the transitional quadrupole moments were deduced. The obtained Q_t for the different bands are compared with total Routhian surface (TRS) calculations and particle-rotor-model calculations. The TRS calculations predict different axial symmetric shapes for the bands built on the $9/2^-[514]$, $7/2^+[404]$, and $1/2^-[541]$ configurations, with a γ softness for the $9/2^-[514]$ configuration. This band has also been studied using the particle-rotor model, the results of which, however, are consistent with a triaxial shape with a γ value of -15°.

DOI: 10.1103/PhysRevC.71.014312 PACS number(s): 21.10.Tg, 21.10.Ky, 27.70.+q

I. INTRODUCTION

Although a variety of different shapes may be found in nuclei, it is difficult to probe deviations from axial symmetry. The Lu ($Z = 71$) isotopes around $A \approx 165$ show evidence of superdeformed triaxial bands [1–4] at high spins, but whether these nuclei also have a stable triaxial shape at normal deformation remains an open question. Analysis of signature splitting suggests that this is in fact the case for the yrast $9/2^-[514]$ band [5,6]. However, signature splitting also occurs in axially symmetric deformed nuclei, due to K mixing. A complementary test for axial asymmetry is to measure the quadrupole moment of the band [7,8]. The quadrupole moments depend on the β as well as the γ deformation; therefore the experimental values must be compared with calculations. To investigate the triaxiality further, an experiment aimed at determining the lifetimes of excited states of ^{165}Lu has been performed. Lutetium-165 represents a good testing ground because of its close-to-yrast bands based on different proton configurations, with possible different shape-driving effects.

II. EXPERIMENT

The reaction used to populate the nucleus of interest was ^{139}La(^{30}Si, $4n$)^{165}Lu at a beam energy of 135 MeV (in the middle of the target). The beam was delivered by the XTU-tandem accelerator of Laboratori Nazionali di Legnaro, Italy. The target material consisted of 1.04 mg/cm^2 ^{139}La, which was evaporated on a 1.4 mg/cm^2 Ta support. It also had a thin gold layer on the other side to prevent oxidation. The target was mounted with the Ta support facing the beam inside the plunger apparatus designed by the University of Cologne [9]; the apparatus was designed specifically for coincidence recoil distance measurements. A thick 6.4 mg/cm^2 Au foil was used as a stopper for the recoiling nuclei after flight in vacuum. The plunger apparatus was mounted in the center of the GASP array [10] in configuration I. In this configuration GASP consists of 40 Compton-suppressed, high-purity Ge γ-ray detectors, with a total photopeak efficiency of 3% at 1.3 MeV, and 80 bismuth germanate (BGO) detectors. The 40 Ge detectors are arranged at seven different angles relative to the beam line (6 at 34°, 6 at 60°, 4 at 72°, 8 at 90°, 4 at 108°, 6 at 120°, and 6 at 146°). Events with at least two Ge detectors firing in coincidence were written to tape. The γ-ray coincidence data were taken at 19 different target-stopper distances between 2 and 7200 μm. The plunger is equipped with a feedback system to correct for thermal shifts of the target-to-stopper separations. This system uses the capacitance between target and stopper

*Corresponding author: K.Andgren@surrey.ac.uk.

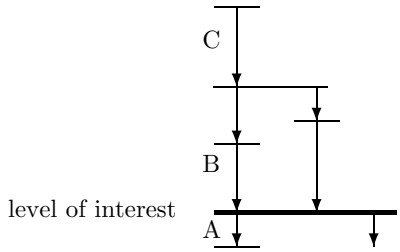

FIG. 1. A schematic level scheme showing the meaning of direct *B* and indirect *C* feeding transitions, as well as the transition following the decay *A*.

foils to generate a feedback signal which is supplied to a piezocrystal.

III. DATA ANALYSIS

A total of 2.5×10^9 events were recorded. For each target-stopper distance and each angular combination, the data were sorted into $\gamma\gamma$-coincidence matrices. This means that a total of $19 \times 7 \times 7 = 931$ matrices were created. The lifetimes were determined using the differential decay curve method (DDCM) [11,12]. A correct application of the DDCM requires γ-ray intensities at different distances. Therefore, all of the matrices were normalized with respect to the total number of counts in each matrix. It was checked that this was proportional to the intensities of some of the strongest peaks in ^{165}Lu. This was done by examining the peak intensities relative to the total number of counts in the matrix for one ring-ring combination (90°-90°) at all of the 19 distances and for all of the ring-ring combinations at one distance (23 μm). The velocity of the recoiling nuclei was obtained by measuring the shifted energies of some of the strongest transitions in ^{165}Lu at the different angles. The measurements gave a value for the velocity of $v = 1.54(3)\%$ of the speed of light.

The DDCM avoided the lifetime uncertainties related to unobserved side feeding and delayed feeding. A gate was set on the shifted component of the feeding transition and the intensities of the shifted and unshifted peaks of the γ ray following the decay (see Fig. 1) were analyzed at the different distances giving mean lives,

$$\tau = \frac{I_u^{BA}}{v\frac{dI_s^{BA}}{dx}}, \tag{1}$$

where I_u is the intensity of the unshifted peak, I_s is the intensity of the shifted peak (both the intensities are taken from spectra when a gate is set on the shifted component of the feeding transition), v is the velocity, and x is the target-stopper distance. The capital-letter indices in the expression, which specify the intensities, are defined in Fig. 1. In some cases, when the direct feeding transition could not be used because of contamination, a gate was set on the shifted component of an indirect feeder. The formula then changed to

$$\tau = \frac{I_u^{CA} - \alpha I_u^{CB}}{v\frac{dI_s^{CA}}{dx}}, \tag{2}$$

where α is the ratio

$$\alpha = \frac{I_u^{CA} + I_s^{CA}}{I_u^{CB} + I_s^{CB}}. \tag{3}$$

For each ring of detectors, a gate was set on one of the axes in the $6 \times 6 \times 19$ coincidence matrices. (The detectors at 90° could not be used because the energies were not Doppler shifted at that angle.) Figure 2 presents examples of γ-ray coincidence spectra.

To increase the statistics, the cuts were then summed up, for each of the six rings, on the second axis. The weighted average of the lifetime was derived by fitting a straight line through the points of the $\tau(x)$ curve calculated using Eq. (1). Only the relevant points in the region of sensitivity, where the intensity curves were steep, were taken into account; see Fig. 3. The lifetimes were checked for each angle to ensure that the spectra contained no contamination. To increase the statistics further, these six sets of spectra were finally, if

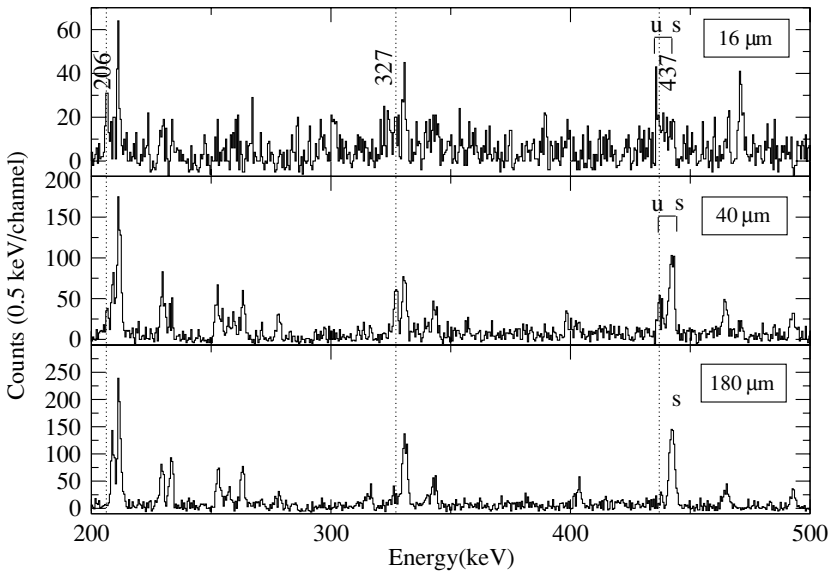

FIG. 2. γ-ray spectra obtained from a gate on the shifted component of the 519 keV transition ($23/2^- \rightarrow 19/2^-$ in the $9/2^-[514]$ band). The shifted and unshifted parts of transitions in the same band are labeled. The ring-ring combination is 34°-34° and the target-stopper distances from top to bottom are 16, 40, and 180 μm.

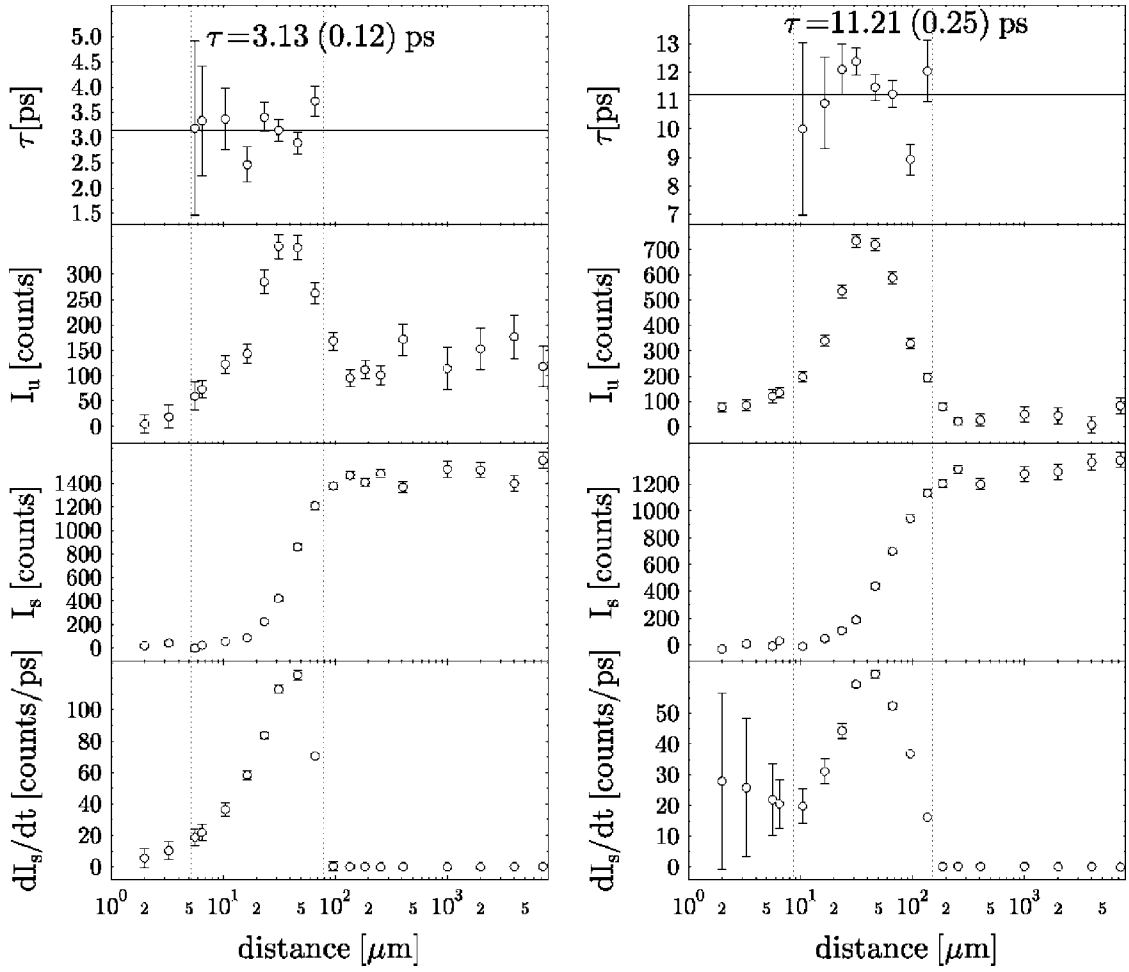

FIG. 3. Lifetime determination of the $I^\pi = 17/2^+$ level of the $7/2^+[404]$ band (left) and the $I^\pi = 17/2^-$ level of the $1/2^-[541]$ band (right). The $\gamma\gamma$ matrices were gated on the shifted components of the feeding transitions 538 and 433 keV, respectively. The intensities of the unshifted and shifted peaks of the decaying 475 and 335 keV transitions are shown in the middle panels. The derivative of the shifted peak is shown in the bottom panels. From this information, the lifetime was extracted and the result is shown in the upper panels. The dotted lines show the region of sensitivity where the lifetimes were determined.

the spectra were free from contamination, summed into one set of spectra (i.e., 19 spectra, one summed spectrum for each distance). Examples of such lifetime determinations are shown in Fig. 3.

In some of the cuts this could not be done because of contaminating transitions, mainly from transitions in the same nucleus. In these cases, only the clean ring-ring combinations were used. Also, if the depopulating γ energy was too low ($\lesssim$200 keV) clean sum-spectra could not be obtained, since the unshifted and shifted peaks were not completely separated. In this case the average value of the lifetimes obtained at different angles was considered instead.

IV. RESULTS

Lifetimes of 19 different states were obtained for four of the rotational bands built upon the $9/2^-[514]$, $7/2^+[404]$, $1/2^-[541]$, and $1/2^+[411]$ single-particle configurations. See Fig. 4 for a partial level scheme of ^{165}Lu. A fifth rotational band built on the $5/2^+[402]$ configuration has also been discovered in this nucleus [13], but this band was weakly populated in the present experiment. The measured lifetimes ranged from $\sim$1 to $\sim$200 ps and are given in Table I together with the extracted reduced transition probabilities $B(E2)$. Higher up in spin, the lifetimes became $\lesssim$1 ps, which was comparable to the slowing down time of the recoil in the stopper, and therefore these lifetimes could not be determined using this method. In general, the lifetimes were determined by gating on the direct feeder, except for the $9/2^-$ state of the $1/2^-[541]$ band where the gate was set on the indirect feeding transition of 433 keV, since the direct feeding transition of 228 keV is a doublet (the partner is in the $7/2^+[404]$ band). It is generally easier to extract clean spectra if the gate is set on a higher energy transition, since there are fewer transitions with higher energy and their shifted and unshifted parts are also more separated. The lifetime of the 15/2+ state in the band built on the $7/2^+[404]$ orbital could not be measured because the 509 keV transition was too close to the electron-positron annihilation γ rays at 511 keV. The same problem resulted

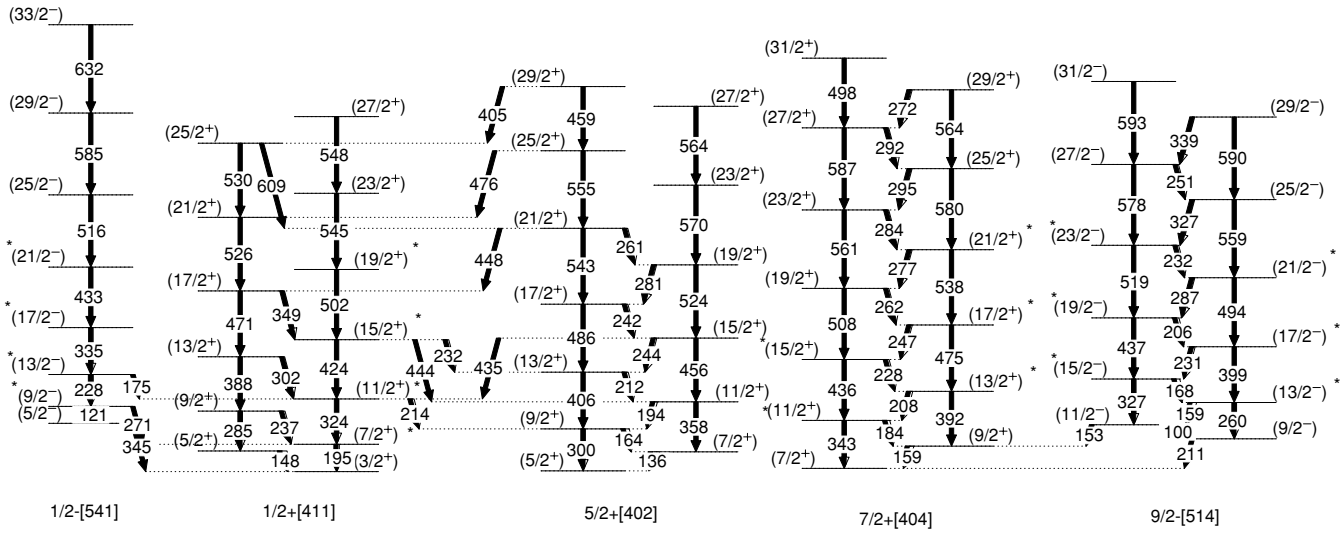

FIG. 4. Partial level scheme of ^{165}Lu, showing the five known rotational bands built on different single-particle orbitals. For a more detailed level scheme see Refs. [3,13,14]. The states for which the lifetimes were extracted are marked with a ⋆.

in a large uncertainty in the lifetime of the $21/2^-$ state of the $K^\pi = 1/2^-$ band.

The accurate branching ratios needed to calculate the $B(E2)$ values were taken from Ref. [14]. The $B(E2)$ value of the $13/2^-$ state in the band built on the $9/2^-[514]$ orbital could not be determined because of difficulties in obtaining the correct branching ratio for the decaying transitions. The mixing ratio parameter $\delta^2 = T_\gamma(E2; J \to J-1)/T_\gamma(M1; J \to J-1)$, where $T_\gamma(E2; J \to J-1)$ and $T_\gamma(M1; J \to J-1)$ are the γ-ray intensities of the $E2$ and $M1$ components, and its effect on the internal conversion coefficient were taken into account. Assuming axial symmetry and that the quadrupole deformation has the same value when extracted from the $B(E2; I \to I-2)$

TABLE I. Measured lifetimes and the calculated transition probabilities and quadrupole moments of excited states in ^{165}Lu. The levels are grouped according to the bands they belong to.

Band	I^π ($\hbar$)	E_x (keV)	τ (ps)	$B(E2; I \to I-2)$ (e^2 b^2)	$Q_t(\gamma = 0°)$[a] (e b)	Q_t^b[b] (e b)	γ[c] (deg)
$9/2^-[514]$	$13/2^-$	494	18.76(86)				
	$15/2^-$	662	9.59(50)	0.64(8)	7.70(49)	5.73(37)	−15
	$17/2^-$	893	4.20(18)	0.65(9)	6.55(43)	5.20(34)	−15
	$19/2^-$	1099	2.45(9)	0.99(8)	7.27(30)	5.96(24)	−15
	$21/2^-$	1386	1.81(26)	0.69(11)	5.69(44)	4.76(36)	−15
	$23/2^-$	1618	1.41(10)	0.96(8)	6.39(27)	5.43(23)	−15
$7/2^+[404]$	$11/2^+$	366	22.70(215)	0.32(4)	6.64(46)		
	$13/2^+$	574	9.67(35)	0.52(5)	6.23(29)		
	$15/2^+$	802	5.28(23)	0.69(5)	6.20(21)		
	$17/2^+$	1049	3.13(12)	0.84(4)	6.26(15)		
	$21/2^+$	1587	1.59(11)	0.86(7)	5.74(22)		
$1/2^-[541]$	$9/2^-$	466	84.64(498)	1.40(26)	7.01(66)		
	$13/2^-$	695	48.02(205)	2.01(11)	8.02(21)		
	$17/2^-$	1030	11.21(25)	1.63(8)	7.05(17)		
	$21/2^-$	1463	4(1)	1.32(33)	6.26(78)		
$1/2^+[411]$	$7/2^+$	195	192.85(1661)	1.03(9)	6.35(28)		
	$11/2^+$	520	21.46(99)	0.85(5)	5.32(15)		
	$15/2^+$	943	2.66(24)	1.13(13)	5.94(34)		
	$19/2^+$	1445	3.12(14)	0.81(4)	4.93(11)		

[a]Calculated using Eq. (4), assuming no triaxiality.

[b]Calculated using Eq. (5) assuming the triaxiality given by the particle-rotor calculations of Ref. [6].

[c]Triaxiality according to the particle-rotor calculations of Ref. [6].

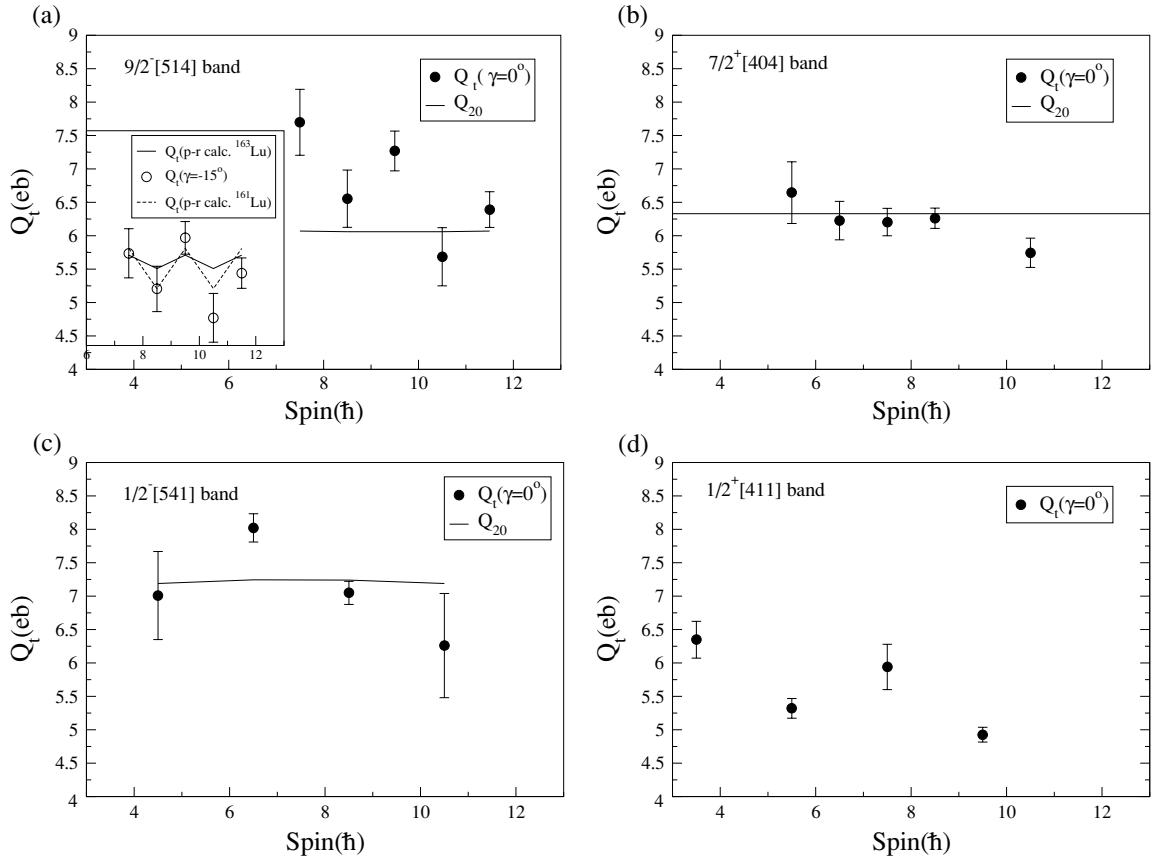

FIG. 5. The transition quadrupole moment plotted versus spin for the rotational bands built on the (a) $9/2^-$, (b) $7/2^+$, (c) $1/2^-$, and (d) $1/2^+$ bands, respectively. The experimental $Q_t(\gamma = 0^\circ)$ and $Q_t(\gamma)$ are marked with filled and unfilled circles. The theoretical Q_{20} values from the TRS calculations are shown as solid lines. It can be seen that Q is different for different rotational bands. In the inset of (a) the experimental Q_t with $\gamma = -15^\circ$ and the theoretically obtained quadrupole moments for ^{161}Lu and ^{163}Lu from the particle-rotor calculations [6] are plotted against spin.

and from the $B(E2; I \to I-1)$ transition probabilities gives the relation $B(E2; I \to I-2)/B(E2; I \to I-1) = [\langle IK20|(I-2)K\rangle/\langle IK20|(I-1)K\rangle]^2$, which was used to extract δ^2. We note that for the bands built on the $9/2^-[514]$ and the $7/2^+[404]$ configurations, the δ^2 mixing ratio has been extracted from angular correlation measurements [13,15]. The estimated δ^2 lies a factor of 2–3 below the measured ones, which might be a consequence of K mixing and/or deviation from axial symmetry. However, the effect on the determined quadrupole moments due to the different δ^2 is smaller (on the order of 1–4 $\times 10^{-2}$ e b) than those caused by other uncertainties. From the reduced transition probabilities, the transitional quadrupole moment, under the assumption of an axially symmetric deformed shape $Q_t(\gamma = 0^\circ)$, was calculated using the relation

$$Q_t^2 = \frac{16\pi}{5} B(E2; I \to I-2) |\langle IK20|(I-2)K\rangle|^{-2}. \quad (4)$$

The obtained transitional quadrupole moments are shown in Table I and in Fig. 5.

V. DISCUSSION

To get a deeper understanding of the nuclear shape, we performed total Routhian surface (TRS) calculations using the nonaxial deformed Woods-Saxon potential [16]. Collective rotation was investigated in the frame of the cranked shell model in the three-dimensional deformation space of β_2, γ, and β_4. Both monopole and double-stretched quadrupole pairings were included [17]. The monopole pairing strength G was determined by the average-gap method [18], and quadrupole pairing strengths were obtained by restoring the Galilean invariance broken by the seniority pairing force [19]. To avoid the spurious phase transition encountered in the BCS approach, we used approximate particle-number projection by means of the Lipkin-Nogami method [20]. Pairing correlations are dependent on the rotational frequency and deformation. In order to include such dependence in the TRS, we performed pairing-deformation-frequency self-consistent TRS calculations; i.e., for any given deformation and frequency, the pairing gaps were self-consistently calculated by a HFB-like method [20]. At a given frequency, the deformation of a state was determined by minimizing the calculated TRS. The calculations indicate no significant shape changes below the

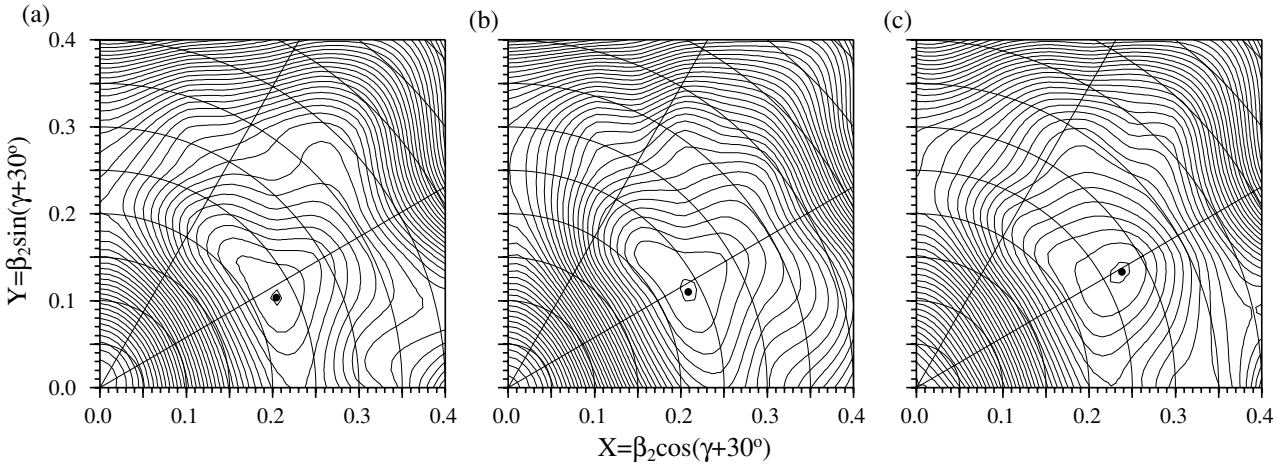

FIG. 6. TRS calculations for different single-particle bands at a rotational frequency of $\hbar\omega = 0.2$ MeV (corresponding to spin $I \approx 7$–$10\,\hbar$). The energy spacing between the contours is 200 keV. (a) The $7/2^+$ [404] band with the energy minimum at $\beta_2 = 0.236$, $\beta_4 = 0.014$, $\gamma = -2.1^\circ$, (b) the $9/2^-$[514] band with the energy minimum at $\beta_2 = 0.229$, $\beta_4 = 0.014$, $\gamma = -3.1^\circ$, and (c) the $1/2^-$[541] band with the energy minimum at $\beta_2 = 0.273$, $\beta_4 = 0.029$, $\gamma = -0.8^\circ$.

backbending; typical TRS plots corresponding to the bands of interest are shown in Fig. 6.

The TRS calculations could not be performed for the second excited $(\pi, \alpha) = (+, -1/2)$ rotational states built on the $1/2^+$[411] bandhead because the present version of the code can block only the lowest lying configuration for a given parity and signature. The TRS values for the four bandheads were also calculated, since the particle configuration could be fixed at spin zero. The difference between the bandhead deformation and the deformation at the relevant spins is between 0 and 6% for the three bands where both calculations are available.

The theoretical intrinsic quadrupole moment was extracted as $Q = \sum 2V_k^2 q_k$, where q_k are the single-proton quadrupole moments obtained from the Wood-Saxon wave functions and V_k^2 are the pairing occupation probabilities of the k:th orbital. The quadrupole moment has contributions from two spherical-tensor components, $Q = Q_{20} + Q_{22}$. The Q_{20} term depends on the β_2 quadrupole deformation and it is independent of the degree of triaxiality. The Q_{22} term vanishes for axially symmetric nuclei, being negative for positive γ, and positive for negative γ deformations. In our case where the predicted $\gamma \approx 0^\circ$ for all the single-particle bands, only the Q_{20} term is considered.

The band based on the $9/2^-$[514] configuration is the yrast band. The TRS calculations predict the energy minima at $\beta_2 = 0.229$, $\beta_4 = 0.014$, $\gamma = -3.1^\circ$, with a γ softness for the negative signature. For positive signature, the lowest configuration in the TRS corresponds to the $1/2^-$[541] orbital and hence we are not able to calculate the TRS for the $9/2^-$[514] configuration. An increasing amount of signature splitting is observed in this band. This might be explained by the γ softness predicted by the TRS calculations for the negative signature, but the result is inconclusive. Also, the quasiproton Routhians show a signature splitting of this band at low spins when triaxiality is assumed. The experimental values might indicate higher quadrupole moments for the negative signature, which supports a triaxial deformation, with negative γ values. There might also be a slight trend of decreasing quadrupole moments with increasing angular momenta. The experimental average (of the five points, two for the positive and three for the negative signature, respectively) quadrupole moment is 6.70(16) e b. The average Q_t for the negative signature only, of 6.92(19) e b, is different from the theoretical one of 6.06 e b. See Fig. 5(a) for a plot of the theoretical and experimentally obtained quadrupole moments.

This band has also been extensively studied using the particle-rotor model [5,6,21]. In those works, the (signature splitting of the) energy spectrum, the $B(M1)/B(E2)$ transition strength ratios, and the experimentally available $Q^{(1)}/Q^{(2)}$ ratios [where $B(E2; \Delta I = p) = \frac{5}{16\pi}\langle I\,K\,20|I-p,\,K\rangle^2 Q^{(p)}$] are fitted. This latter ratio is very sensitive to the γ deformation and nearly independent of β: $\mathrm{Q}^{(1)}/Q^{(2)} \sim \cos(30^\circ - \gamma)/\cos(30^\circ + \gamma)$. These calculations indicate a significant triaxiality for the odd-Z ^{161,163,165,167}Lu isotopes, with increasing γ deformation as the neutron number decreases. In particular, for the ^{165}Lu nucleus, $\gamma = -19^\circ$ and $\gamma = -15^\circ$ were suggested by [5] and [6] respectively. Similar conclusions are drawn in Ref. [22] for the case of the tantalum isotopes (with $\gamma = -18^\circ$ for ^{165}Ta). In the last columns of Table I the experimentally extracted quadrupole moments assuming the deformation parameter $\gamma = -15^\circ$ are given using the formula [23],

$$Q_t^2 = \frac{8\pi}{5} B(E2; I \to I-2) \frac{(2I-1)(2I+1)}{(I-1)I} \times \left[\cos(\gamma + 30^\circ) - \cos(\gamma - 30^\circ)\frac{K^2}{(I-1)I}\right]^{-2} \quad (5)$$

In the inset of Fig. 5(a), these values are compared with the theoretical ones for ^{161}Lu and ^{163}Lu [6] (no values for ^{165}Lu are published), which suggests $Q_t \approx 5.8$ and 5.7 e b for negative signature and $Q_t \approx 5.2$ and 5.5 e b for positive signature for ^{161}Lu and ^{163}Lu respectively. There is a remarkable agreement between the particle-rotor model and the experiment.

In the case of the $7/2^+[404]$ band, the two signatures are predicted to have similar deformations with $\beta_2 = 0.236$, $\beta_4 = 0.014$, and $\gamma = -2.1^\circ$. The constant nature of the extracted quadrupole moments is consistent with this. The average of the experimental quadrupole moments of 6.16(10) e b is slightly lower than the theoretical value of 6.33 e b.

It is expected that the band based on the $1/2^-[541]$ configuration has the highest deformation because of the strong core-polarizing effect of this Nilsson orbital. Jónsson *et al*. [13] needed to consider higher deformation compared to the $9/2^-[514]$, $7/2^+[404]$, $1/2^+[411]$ configurations in order to reproduce the crossing frequencies (alignment of $i_{13/2}$ neutron pair) in the cranked shell model calculations. This is consistent with the experimental observations in $^{165}_{69}$Tm, where it was found that the quadrupole moment of the $1/2^-[541]$ band is 15% higher than that of the $7/2^+[404]$ and $1/2^+[411]$ bands [24]. Our TRS calculations predict a higher deformation for this band than for the $7/2^+$ and $9/2^-$ bands, namely, $\beta_2 = 0.273$, $\beta_4 = 0.029$, and $\gamma = -0.8^\circ$. In accordance with this, the experimental average quadrupole moment $Q_t = 7.39(13)$ e b is higher than in the other three bands.

In the case of the $1/2^+[411]$ band no TRS calculations for the relevant spins could be performed. Instead the bandhead deformation was calculated and the deformation parameters were determined: $\beta_2 = 0.232$, $\beta_4 = 0.016$, $\gamma = 2.2^\circ$, with a rather γ-soft shape. The experimentally obtained quadrupole moments suggest a reduction of deformation with increasing angular momentum. The theoretical value of 6.86 e b (calculated using the β values from the TRS) for the $I^\pi = 1/2^+$ bandhead fits well into this trend.

VI. CONCLUSIONS

A fusion-evaporation reaction experiment has been performed in order to populate medium spin states in ^{165}Lu. A total of 19 lifetimes in four rotational bands have been measured for the first time by means of the differential decay curve method. The extracted transition strengths and transition quadrupole moments were compared with theoretical calculations. There is general agreement between the experimental data and the performed TRS calculations, which give axially deformed shapes for the $9/2^-[514]$, $7/2^+[404]$, and $1/2^-[541]$ bands, with a γ softness for the $9/2^-[514]$ configuration. Within this theory the differences in quadrupole moments are explained by different axial symmetric shapes, with the $1/2^-[541]$ band being the most deformed. It is not clear from the calculations whether the observed signature splitting in the $9/2^-[514]$ band could be explained by the predicted γ softness. On the other hand, the quadrupole moments obtained for the $9/2^-[514]$ band are in remarkably good agreement with previous particle-rotor calculations [5,6]. These calculations, in contrast to the TRS calculations, are consistent with a considerable amount of triaxiality ($\gamma = -15^\circ$).

ACKNOWLEDGMENTS

The authors thank the staff of the tandem accelerator, Legnaro, for providing a high-quality beam. This work was supported by EPSRC(UK) and the EU (Contract No. HPRI-CT-1999-00083). Zs. P. acknowledges the receipt of an EPSRC Advanced Fellowship Award (GR/A10789/01).

[1] G. Schönwaßer *et al*., Phys. Lett. **B552**, 9 (2003).
[2] W. Schmitz, C. X. Yang, H. Hübel, A. P. Byrne, R. Müsseler, N. Singh, K. H. Maier, A. Kuhnert, and R. Wyss, Nucl. Phys. **A539**, 112 (1992).
[3] H. Schnack-Petersen *et al*., Nucl. Phys. **A594**, 175 (1995).
[4] C. Y. Yang *et al*., Eur. Phys. J. A **1**, 237 (1998).
[5] I. Hamamoto and H. Sagawa, Phys. Lett. **B201**, 415 (1988).
[6] Yu-sheng Liang, Xing-ju Wu, Jin-zhang Xu, Xing-qu Chen, and Zheng Xing, Phys. Rev. C **60**, 054305 (1999).
[7] Zs. Podolyák *et al*., Phys. Rev. C **66**, 011304 (2002).
[8] P. Petkov *et al*., Phys. Rev. C **63**, 014304 (2000).
[9] A. Dewald *et al*., in *Proceedings of the Seminar on Nuclear Physics with Radioactive Ion Beam and High Spin Nuclear Structure, Lanzhou, China,* edited by G. Jin, Y. Lou, W. Zhan (Atomic Energy Press, Lanzhou, China, 1998), p. 31.
[10] D. Bazzacco, in Proceedings of the International Conference on Nuclear Structure at High Angular Momentum, Ottawa, 1992, Chalk River Report No. AECL 10613, 1982 (unpublished), p. 386.
[11] A. Dewald, S. Harissopulos, and P. von Brentano, Z. Phys. A **334**, 163 (1989).
[12] G. Böhm, A. Dewald, P. Petkov, and P. von Brentano, Nucl. Instr. Methods Phys. Res. **A329**, 248 (1993).
[13] S. Jónsson *et al*., Nucl. Phys. **A422**, 397 (1984).
[14] G. Schönwaßer *et al*., Nucl. Phys. **A735**, 393 (2004).
[15] P. Frandsen *et al*., Nucl. Phys. **A489**, 508 (1988).
[16] W. Nazarewicz, J. Dudek, R. Bengtsson, T. Bengtsson, and I. Ragnarsson, Nucl. Phys. **A435**, 397 (1985).
[17] W. Satuła and R. Wyss, Phys. Rev. C **50**, 2888 (1994); Phys. Script. T **56**, 159 (1995).
[18] P. Möller and J. R. Nix, Nucl. Phys. **A536**, 20 (1992).
[19] H. Sakamoto and T. Kishimoto, Phys. Lett. **B245**, 321 (1990).
[20] W. Satuła, R. Wyss, and P. Magierski, Nucl. Phys. **A578**, 45 (1994).
[21] I. Hamamoto and B. R. Mottelson, Phys. Lett. **B167**, 370 (1986).
[22] M. S. Fetea and R. F. Fetea, Nucl. Phys. **A690**, 239 (2001).
[23] P. Petkov *et al*., Nucl. Phys. **A640**, 293 (1998).
[24] H. J. Jensen *et al*., Nucl. Phys. **A695**, 3 (2001).